Remote Sensing of Environment 136 (2013) 135–145

Contents lists available at SciVerse ScienceDirect

Remote Sensing of Environment

journal homepage: www.elsevier.com/locate/rse

A Simplified high resolution MODIS Aerosol Retrieval Algorithm (SARA) for use over mixed surfaces

Muhammad Bilal [a], Janet E. Nichol [a,*], Max P. Bleiweiss [b], David Dubois [c]

[a] Department of Land Surveying & Geo-Informatics, The Hong Kong Polytechnic University, Hung Hom, Kowloon, Hong Kong
[b] Center for Applied Remote Sensing in Agriculture, Meteorology, and Environment, Department of Entomology, Plant Pathology, and Weed Science, New Mexico State University, Las Cruces, NM, USA
[c] Department of Plant and Environmental Sciences, New Mexico State University, Las Cruces, NM, USA

ARTICLE INFO

Article history:
Received 18 October 2012
Received in revised form 19 April 2013
Accepted 20 April 2013
Available online xxxx

Keywords:
AERONET
MODIS
AOD
New simplified algorithm
500 m resolution
Hong Kong

ABSTRACT

Aerosol Optical Depth (AOD) is a measure of the columnar atmospheric aerosol content. Satellite remote sensing has been used to retrieve AOD over land and ocean at spatial resolutions of several to several tens of km. In most cases, a Radiative Transfer Model (RTM) is used to construct a look-up table (LUT) to act as a map between measurements and physical quantities. In the current study, MODerate resolution Imaging Spectroradiometer (MODIS) measurements were used to develop a Simplified Aerosol Retrieval Algorithm (SARA) for use over Hong Kong at high (500 m) spatial resolution, without using a LUT. Instead, RTM calculations were applied directly to the MODIS data, with the aerosol properties derived from a local urban Aerosol Robotic Network (AERONET) station at the Hong Kong Polytechnic University, and surface reflectance from the MOD09GA level-2 daily surface reflectance product. For validation, the SARA AOD at 500 m, along with the operational MODIS aerosol product (MOD04 C005) at 10 km spatial resolution, was compared with data from a ground-based Microtops II sun photometer at the Hong Kong International Airport, a Sky-radiometer at the City University of Hong Kong, and an AERONET station at Hong Kong Hok Tsui. The 500 m AOD retrieved from the SARA showed a high consistency with ground-based AOD measurements, with average correlation coefficient ~0.964, root mean square error (RMSE) ~0.077, and mean absolute error (MAE) ~0.065. The SARA AOD showed a good agreement with MOD04 C005 AOD over both urban and rural areas of Hong Kong, with average correlation coefficient ~0.917, RMSE ~0.087, and MAE ~0.072. The results demonstrate that our simplified AOD algorithm is better able to represent aerosol conditions over Hong Kong than the MOD04 C005 standard product as well as other higher resolution algorithms which have been tested over Hong Kong.

1. Introduction

Atmospheric aerosols are particles suspended in the atmosphere that vary in their size distribution, shape, total column content, and composition (Kaufman et al., 1997a). Aerosols play an important role in determining the earth's radiation budget and its impact on climate variability by the scattering and absorption of incoming solar energy. They also absorb incoming solar radiation which causes a warming effect in the atmosphere, whereas aerosol forcing at the top of the atmosphere may cause a cooling effect by reflecting solar radiation. A full understanding of the impact of aerosol particles in climate and air quality control strategies requires the retrieval of aerosol amounts and characteristics. Spectral aerosol optical depth (AOD) is the parameter most frequently used, because it is the easiest quantitatively-useful parameter to obtain (Clarke et al., 2001; Holben et al., 2001). AOD is a measure of the extinction (scattering + absorption) of solar light due to aerosol particles (Ångström, 1930; van de Hulst, 1948). Satellite remote sensing with passive imaging radiometers can provide quantitative measurements of AOD (Tang et al., 2005) from local to global scales (Kaufman et al., 2002). The spatial variability of AOD can be examined much better from satellite sensors than from ground stations, but satellite retrieval is subject to four major uncertainties/challenges: calibration, cloud screening, selection of the aerosol model and correction for surface reflection (Li et al., 2009).

Over land, the main objective of satellite remote sensing is to retrieve aerosol optical properties between the top of the atmosphere (TOA) and the ground surface, as satellite received radiation corresponds to radiation reflected from the surface affected by atmospheric and aerosol scattering along the path as well as atmospheric path radiance. Since this path radiance from the atmosphere corresponds to the optical penetration of light or AOD, the estimation of surface reflectance (Li et al., 2009; Mishchenko et al., 1999) is an important factor in developing an aerosol retrieval algorithm over land. Low surface reflectance values allow good discrimination between path radiance of aerosols and the radiance of the land surface. However, high surface

* Corresponding author. Tel.: +852 2766 5952; fax: +852 2330 2994.
E-mail address: lsjanet@inet.polyu.edu.hk (J.E. Nichol).

0034-4257/$ – see front matter © 2013 Elsevier Inc. All rights reserved.
http://dx.doi.org/10.1016/j.rse.2013.04.014

reflectance values make it difficult to accomplish this discrimination as aerosol path radiance is often lower than surface radiance. AOD products over land can be obtained by sensors such as the Total Ozone Mapping Spectrometer (TOMS, Torres et al., 2002), the Sea-viewing Wide Field-of-view Sensor (SEAWIFS, Sayer et al., 2012), the Ozone Monitoring Instrument (OMI, Torres et al., 2007), Polarization and Directionality of the Earth's Reflectances (POLDER, Herman et al., 1997), the Along Track Scanning Radiometer (ATSR-2, North, 2002), the Geostationary Operational Environmental Satellite (GOES, Prados et al., 2007), the Advanced Very High Resolution Radiometer (AVHRR, Hauser et al., 2005; Riffler et al., 2010), the MEdium Resolution Imaging Spectroradiometer (MERIS, Vidot et al., 2008), the Multiangle Imaging SpectroRadiometer's (MISR, Kahn et al., 2005, 2010), and AOD is available as standard products from the MOderate Resolution Imaging Spectroradiometer (MODIS) deep blue algorithm (Hsu et al., 2004, 2006) and dark target algorithm (Levy et al., 2007a, 2010; Remer et al., 2005, 2008).

MODIS sensors aboard the National Aeronautics and Space Administration (NASA)'s Earth Observing System (EOS) satellite platforms, Terra and Aqua, have operated since December 1999 and May 2002 respectively. Terra is a polar orbiting satellite at an altitude of approximately 700 km with equatorial crossing (southward) at around 10:30 a.m. local solar time (LST), and a swath width of 2330 km. MODIS has 36 wavelength channels ranging from 0.41 to 14 μm at moderate spatial resolutions (250m, 500 m and 1 km) and good temporal resolution (1 to 2 days). It retrieves AOD over land with spatial resolution of 10 × 10 km at nadir and 20 × 40 km at the edge of the swath. Levy et al. (2007a, 2007b) introduced a "second generation" dark target algorithm, Collection 5 (C005), in the current MOD04 aerosol product. In C005, the surface reflectance relationship between visible and SWIR channels is presented as a function of vegetation index ($NDVI_{SWIR}$) and scattering angle (Levy et al., 2007a). The MODIS algorithm reports Quality Assurance (QA) flags ranging from 3 (good quality) to 0 (poor quality) (Hubanks et al., 2012; Levy et al., 2010). Those with QA flag = 3 provide the best match with AERONET AOD and are strongly recommended for use in quantitative analysis. The C005 dark-target algorithm has been studied globally and regionally (Hyer et al., 2011; Jethva et al., 2007; Levy et al., 2010; Li et al., 2007; Mi et al., 2007; Papadimas et al., 2009), and higher accuracy is reported than for the C004 algorithm. For C005 AOD with QA flag = 3, 72% of retrievals fall within the Expected Error (EE) envelope of $\pm(0.05 + 0.15AOD_{AERONET})$ on a global scale (Levy et al., 2010) but this varies regionally due to different surface types and aerosol loadings. The C005 retrieval is best matched with AERONET AOD where $\rho_{2.21\ \mu m}$ ~ 0.10–0.15 (moderately dark) and $NDVI_{SWIR}$ ~ 0.30–0.40 (moderately green) but it overestimates and underestimates AOD (by 0.02 or more) over bright surfaces ($\rho_{2.21\ \mu m}$ approaching 0.25 and $NDVI_{SWIR} < 0.2$) and unusually dark surfaces ($\rho_{2.21\ \mu m} < 0.05$ or green at $NDVI_{SWIR} > 0.6$), respectively (Levy et al., 2010). The C005 retrieval has a positive bias in AOD due to cloud fraction which varies from 26% of "Bad (QA flag = 0)" retrievals to 10% of "Very Good (QA flag = 3)" retrievals (Hyer et al., 2011).

Monitoring and understanding the behavior of atmospheric aerosols at local scales over complex urban terrain such as Hong Kong requires aerosol retrieval algorithms that support high spatial resolution. Thus Li et al. (2005) modified the DDV algorithm to retrieve AOD from MODIS at a 1 km spatial resolution over Hong Kong although validation was limited to DDV dark targets. Wong et al. (2011) retrieved AOD from MODIS at 500 m resolution over Hong Kong using the Minimum Reflectance Technique (MRT) for surface reflectance estimations. However the MRT computation is time consuming and suffers from changing surface reflectance. Wang et al. (2012) retrieved AOD from MODIS at 500 m resolution over Mainland China and Hong Kong using Xue and Cracknell's (1995) surface reflectance estimation method which is based on multiple view-angle observations and a radiative transfer equation, but validation was limited to only two months of data. All of these methods make use of a look-up table (LUT), which includes parameters such as solar and view angles, AOD, single scattering albedo (SSA), asymmetry factor and aerosol models. The MODIS AOD retrieved from the LUT process for the current period is based on viewing geometry and aerosol conditions from earlier observations so that an independent determination is not made. Therefore a new, high spatial resolution satellite aerosol retrieval algorithm based on real viewing geometry encompassing a wide range of aerosol conditions and aerosol types (ω_o = 0.80–1.0) is required to retrieve AOD.

The primary objectives of this study are to: (i) explore a simplified, high resolution AOD retrieval method for MODIS images over mixed surfaces which does not require a LUT, and (ii) evaluate the MOD04 C005 standard aerosol product at 10 km spatial resolution over the same surfaces for comparison purposes. Secondary objectives are to (i) evaluate the ability of the method to identify pollution sources at regional scale, and (ii) analyze the temporal behavior of aerosols over the complex and hilly terrain of Hong Kong.

2. Study area and data used

Hong Kong is situated on complex and hilly terrain on the coast of south-east China with an area of 1095 km^2 and highest elevation of 957 m above sea level. It has a humid subtropical climate with mean annual rainfall from 1400 mm to 3000 mm. It has been experiencing visibility and air quality problems as have many other Asian cities (Chan & Yao, 2008) due to the presence of ambient particulate matter (PM). The PM comes from both local and regional sources (Tsang et al., 2008). To help monitor this situation, two AERONET (urban and rural) stations as well as a Sky-radiometer and Microtops II Sun photometers have been deployed. The Urban AERONET station (Hong_Kong_PolyU, 22.303° N, 114.179° E) is at the center of the urban area at the Hong Kong Polytechnic University (PolyU) and has operated since 2005. The Rural AERONET station (Hong_Kong_Hok_Tsui, 22.209° N, 114.258° E) was installed in a remote rural area near the coast and operated from 2007 to 2010. AERONET (Holben et al., 1998, 2001) is a worldwide network of approximately more than 700 well calibrated Sun photometers. It provides cloud free AOD observations (Smirnov et al., 2000) in seven channels (0.340–1.020 μm) every 15 min, with an uncertainty of ~0.01–0.02 (Holben et al., 2001), which is three to five times more accurate than satellite observations (Remer et al., 2009).

The Microtops II Sun photometer (Morys et al., 2001) is a portable manually operated instrument which was deployed at the Hong Kong Internal Airport (HKIA, 22.317°N, 113.917°E) thought to be the most polluted area of Hong Kong. The Microtops II Sun photometer measures AOD by direct solar irradiance measurements in five wavebands (0.380–1.020 μm) with an uncertainty of ~0.015–0.02 (Knobelspiesse et al., 2004).

The portable ground-based Sky-radiometer is a scanning spectral radiometer (Nakajima et al., 1996) deployed at the City University of Hong Kong (CityU, 22.340°N, 114.170°E) in a suburban area. It measures AOD in five channels (0.400–1.020 μm) by taking measurements of direct and diffuse solar irradiance with an uncertainty of 0.01–0.025 (Campanelli et al., 2004). The Sky-radiometer AOD has differences of 0.01 (Che et al., 2008) to 0.03 (Liu et al., 2011) compared with AERONET AOD.

The PolyU (urban) AERONET AOD at 0.55 μm was used in the development of the SARA, and for validating the retrievals the Hok Tsui (rural) AERONET, CityU (suburban) Sky-radiometer, and HKIA (rural) Microtops II Sun photometers were used. The AOD at 0.55 μm for these instruments was interpolated from other wavelengths using the Ångström exponent (Ångström, 1964). The locations of the AERONET,

Sky-radiometer and Microtops II Sun photometers station in Hong Kong are shown in Fig. 1 and the characteristics of these Sun photometers are given in Table 1.

Remote sensing of aerosols in Hong Kong is limited by cloud cover, but cloud-free skies are most common in November, December and January. The MODIS (Terra) data products (MOD02HKM calibrated radiance, MOD03 geolocation data, MOD09 surface reflectance and MOD04 C005 operational aerosol product) for Hong Kong were obtained from the GSFC (Goddard Space Flight Center) Level 1 and Atmosphere Archive and Distribution System (LAADS) (http://ladsweb.nascom.nasa.gov).

Table 1
AERONET, Sky-radiometer, and Microtops II Sun photometers.

Instrument	AERONET	Sky-radiometer	Microtops II
Wavelength (μm)	0.340	0.440	0.340
	0.380	0.500	0.500
	0.440	0.675	0.675
	0.500	0.870	0.870
	0.675	1.020	1.020
	0.870		
	0.940		
Uncertainty	0.01–0.02	0.01–0.025	0.015–0.02
Field-of-view (°)	1.2	1.0	2.5

3. Methodology

A Simplified Aerosol Retrieval Algorithm was developed that does not use the common technique of constructing a LUT from the Radiative Transfer Model (RTM). Instead, RTM equations were applied directly to the MODIS data products (MOD02, MOD03, and MOD09) to retrieve AOD at high spatial resolution (500 m). The SARA AOD retrievals have three assumptions; (i) the surface is Lambertian, (ii) single scattering approximation, and (iii) the single scattering albedo and asymmetric factor do not vary spatially over the region on day of retrieval. Thus the SARA requires MOD02HKM data to calculate the TOA reflectance, MOD03 data to obtain the solar and view angles, MOD09GA to retrieve the daily surface reflectance and AERONET data to obtain the single scattering albedo and asymmetric factor for the day of the retrieval (the PolyU AERONET station is used for this purpose).

The MOD02HKM swath data provide the satellite received TOA radiance ($L_{TOA(\lambda)}$) in the visible to mid-infrared wavelengths of the solar spectrum from 0.41 μm to 2.16 μm (Salomonson et al., 2006). The SARA is based on the satellite received spectral reflectance (ρ_λ), which is a function of measured spectral radiance ($L_{TOA(\lambda)}$), solar zenith angle, earth–sun distance in astronomical unit and mean solar exoatmospheric radiation (Eq. 1):

$$\rho_{TOA(\lambda)} = \frac{\pi L_{TOA(\lambda)} d^2}{ESUN_\lambda \mu_s} \quad (1)$$

where $\rho_{TOA(\lambda)}$ = satellite received TOA spectral reflectance, $L_{TOA(\lambda)}$ = satellite received TOA spectral radiance, $ESUN_\lambda$ = mean solar exoatmospheric radiation as a function of MODIS band number (Tasumi et al., 2008), d = the earth–sun distance in astronomical unit (Duffie & Beckman, 1991), and μ_s = cosine of solar zenith angle. The satellite received TOA spectral reflectance is defined as a function of atmospheric path reflectance (scattering of solar radiation within the atmosphere), and surface function (reflection of the solar radiation from the surface that is directly transmitted to the TOA). The TOA spectral reflectance, $\rho_{TOA(\lambda)}$, a function of solar and view zenith and azimuth angles, can be estimated using Eq. (2) (Tanré et al., 1988; Vermote et al., 1997):

$$\rho_{TOA(\lambda,\theta_s,\theta_v,\phi)} = \rho_{Aer(\lambda,\theta_s,\theta_v,\phi)} + \rho_{Ray(\lambda,\theta_s,\theta_v,\phi)} + \frac{T_{(\theta_s)} T_{(\theta_v)} \rho_{S(\lambda,\theta_s,\theta_v,\phi)}}{1-\rho_{S(\lambda,\theta_s,\theta_v,\phi)} S_{(\lambda)}} \quad (2)$$

where θ_s = solar zenith angle, θ_v = view zenith angle, ϕ = relative azimuth angle, $\rho_{Aer(\lambda,\theta_s,\theta_v,\phi)}$ = aerosol reflectance resulting from multiple scattering in the absence of molecules, $\rho_{Aer(\lambda,\theta_s,\theta_v,\phi)}$ = Rayleigh reflectance resulting from multiple scattering in the absence of aerosols, $T_{(\theta_s)}$ = transmission of the atmosphere on sun-surface path, $T_{(\theta_v)}$ = transmission of the atmosphere on the surface-sensor path, $\rho_{S(\lambda,\theta_s,\theta_v,\phi)}$ = surface reflectance, and $S_{(\lambda)}$ = atmospheric backscattering

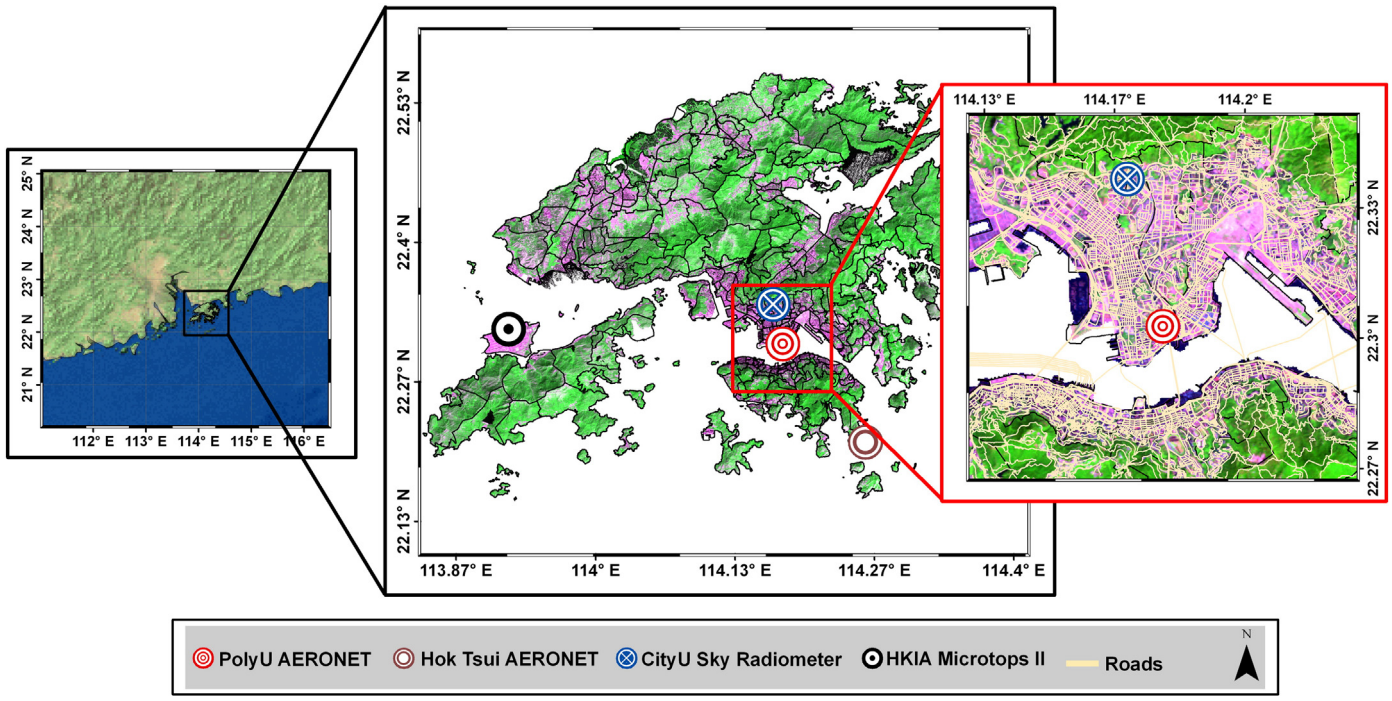

Fig. 1. AERONET, Sky-radiometer and Microtops II Sun photometers station in the complex terrain of Hong Kong.

ratios to account for the multiple reflection between the surface and atmosphere. $T_{(\theta_s)}$ and $T_{(\theta_v)}$ are defined by Eqs. (3) and (4):

$$T_{(\theta_s)} = \exp\left[-(\tau_R+\tau_a) * {}^{1}\!/_{\mu_s}\right] \tag{3}$$

$$T_{(\theta_v)} = \exp\left[-(\tau_R+\tau_a) * {}^{1}\!/_{\mu_v}\right]. \tag{4}$$

Our SARA relies on the aerosol reflectance, $\rho_{Aer(\lambda,\theta_s,\theta_v,\phi)}$, which can be calculated by subtracting the Rayleigh path reflectance, $\rho_{Ray(\lambda,\theta_s,\theta_v,\phi)}$, and surface function from the satellite measured top of atmosphere reflectance, $\rho_{TOA(\lambda,\theta_s,\theta_v,\phi)}$ (Eq. 5):

$$\rho_{Aer(\lambda,\theta_s,\theta_v,\phi)} = \rho_{TOA(\lambda,\theta_s,\theta_v,\phi)} - \rho_{Ray(\lambda,\theta_s,\theta_v,\phi)} - \frac{T_{(\theta_s)}T_{(\theta_v)}\rho_{s(\lambda,\theta_s,\theta_v,\phi)}}{1-\rho_{s(\lambda,\theta_s,\theta_v,\phi)}S_{(\lambda)}}. \tag{5}$$

The correction of the satellite data for Rayleigh scattering (Antoine & Morel, 1998) depends on determination of the Rayleigh phase function (Lado-Bordowsky & Naour, 1997; Liang, 2005) and Rayleigh optical depth (τ_R, Eq. 6, Liang, 2005):

$$\tau_R = \frac{P_z}{P_o}\left(0.00864 + 6.5 * 10^{-6} * z\right)\lambda^{-\left(3.196+0.074\lambda+{}^{0.05}\!/_{\lambda}\right)} \tag{6}$$

where P_z = ambient pressure with respect to elevation (mbar), P_o = 1013.25 mbar (pressure at sea-level), z = ground elevation (height) above sea level in kilometer (km), and λ = wavelength in micrometers.

Surface reflectance is possibly the most important factor in the retrieval of aerosol optical depth from satellite remote sensing measurements (Li et al., 2009; Mishchenko et al., 1999). Surface reflectance for SARA is obtained from the MODIS level-2G (MOD09GA) daily surface reflectance product at 500 m spatial resolution (Vermote & Kotchenova, 2008). This product employs atmospheric correction (conversion of TOA into surface reflectance) to estimate the surface reflectance in MODIS bands 1 to 7 (0.470 μm–2.13 μm). The algorithm used by the MODIS atmospheric products (MOD04 — aerosol optical depth, MOD05 — water vapor, MOD07 — ozone and MOD35 — cloud mask) and ancillary data (Digital Elevation Model (DEM) and Atmospheric Pressure) account for aerosol and gaseous scattering and absorption, adjacency effects of land cover, Bidirectional Reflectance Distribution Function (BRDF) effect, and contamination by thin cirrus. The accuracy of the surface reflectance product (MOD09) depends on the accuracy of these input parameters and is given as 93% and 90% when surface reflectances are 0.3 and 0.1, respectively (Vermote & Kotchenova, 2008). Our SARA algorithm uses the green wavelength (0.55 μm, band 4), of MOD09GA directly.

The Eddington method (Eq. 7) can be used as a good approximation of the atmospheric backscattering ratio (S_λ, Tanré et al., 1979) for the correction of the surface function.

$$S_\lambda = (0.92\tau_R + (1-g)\tau_a)\exp[-(\tau_R+\tau_a)]. \tag{7}$$

The remotely sensed aerosol reflectance, $\rho_{Aer(\lambda,\theta_s,\theta_v,\phi)}$, was retrieved for the 0.55 μm wavelength by correction for Rayleigh scattering $\rho_{Ray(\lambda,\theta_s,\theta_v,\phi)}$ and the surface function. In the single scattering approximation, satellite measured aerosol reflectance is proportional to the aerosol optical depth τ_a, single scattering albedo ω_o and aerosol scattering phase function P_a (Eq. 8, Gordon & Wang, 1994; Kaufman et al., 1997b; King et al., 1999; Kokhanovsky & Leeuw, 2009).

$$\rho_{Aer(\lambda,\theta_s,\theta_v,\phi)} = \frac{\omega_o\tau_{a,\lambda}P_{a(\theta_s,\theta_v,\phi)}}{4\mu_s\mu_v}. \tag{8}$$

Therefore, AOD, τ_a, can be retrieved by re-arranging Eq. (8) as Eq. (9):

$$\tau_{a,\lambda} = \frac{4\mu_s\mu_v}{\omega_o P_{a(\theta_s,\theta_v,\phi)}}\rho_{Aer(\lambda,\theta_s,\theta_v,\phi)}. \tag{9}$$

The aerosol scattering phase function $P_{a(\theta_s,\theta_v,\phi)}$ represents the angular distribution of light scattered by particles and can be determined using the single-term Henyey–Greenstein method (Eq. 10, Rahman et al., 1993):

$$P_{a(\theta_s,\theta_v,\phi)} = \frac{1-g^2}{\left[1+g^2-2g\cos(\pi-\Theta)\right]^{3/2}} \tag{10}$$

where Θ is the scattering phase angle (Levy et al., 2007b). The asymmetry parameter g indicates the relative dominance of forward/back scattering and it remains constant for the most of the aerosol models (Tanré et al., 1979).

Substituting Eq. (5) into Eq. (9) yields Eq. (11) where the three unknowns ($\tau_{a,\lambda}$, ω_o, and g) are shown explicitly. The values of ω_o, and g for the day for which the SARA AOD is being retrieved are determined from a match between SARA AOD as a function of ω_o, and g and the PolyU (urban) AERONET AOD within ±30 min of the MODIS local overpass time. This is accomplished empirically using the fixed point iteration (FPI) method (Kelley, 1995) and by varying the values of ω_o, and g until the match is obtained.

$$\tau_{a,\lambda} = \frac{4\mu_s\mu_v}{\omega_o P_{a(\theta_s,\theta_v,\phi)}}\left[\rho_{TOA(\lambda,\theta_s,\theta_v,\phi)} - \rho_{Ray(\lambda,\theta_s,\theta_v,\phi)} - \frac{e^{-\left(\tau_{R+}\tau_{a,\lambda}\right)/\mu_s}\, e^{-\left(\tau_{R+}\tau_{a,\lambda}\right)/\mu_v}\rho_{s(\lambda,\theta_s,\theta_v,\phi)}}{1-\rho_{s(\lambda,\theta_s,\theta_v,\phi)}\left(0.92\tau_R+(1-g)\tau_{a,\lambda}\right)\exp\left[-\left(\tau_R+\tau_{a,\lambda}\right)\right]}\right]. \tag{11}$$

For validation, AOD measurements from three ground-based Sun photometers were used. Due to limited coincident Sun photometer and MODIS data due to cloud cover and in order to increase the number of statistical samples and also to consider the spatial variability imposed by atmospheric motion, the Sun photometer AOD was averaged within ±30 min (AERONET), and ±60 min (Microtops II sun photometers and Sky-radiometer) of the MODIS overpass time over Hong Kong, and the 500 m retrieved (SARA) AOD was extracted from a 3 × 3 spatial subset region (average of 9 pixels) centered on the ground-based stations (Ichoku et al., 2002). A total of 42, 32 and 20 data points of SARA retrieved AOD for 2007 to 2009 were matched with Hok Tsui AERONET, Sky-radiometer and Microtops II Sun photometers, respectively. The MOD04 C005 AOD from the parameter 'Optical_Depth_Land_and_Ocean (AOD at 0.55 μm for both ocean (best) and land (corrected) with best quality data, QA flag = 3)' was extracted for a 3 × 3 spatial subset region (average of 9 pixels). For C005 AOD, only 16, 42, and 8 values were found to be matched for comparison against AERONET (Fig. 2b), Sky-radiometer (Fig. 4c), and Microtops II (Fig. 4d) Sun photometers, respectively. Finally, the SARA AOD was compared with C005 AOD to evaluate the quality of the SARA retrieval over nine locations of Hong Kong within different land cover types (Table 2).

4. Statistical analysis

Statistical indicators were used to evaluate comparisons of the satellite retrieved AOD with ground-based Sun photometers; namely correlation coefficient (R), root mean square error (RMSE), mean absolute error (MAE), expected error (EE) of AOD, and fraction of EE (FOE).

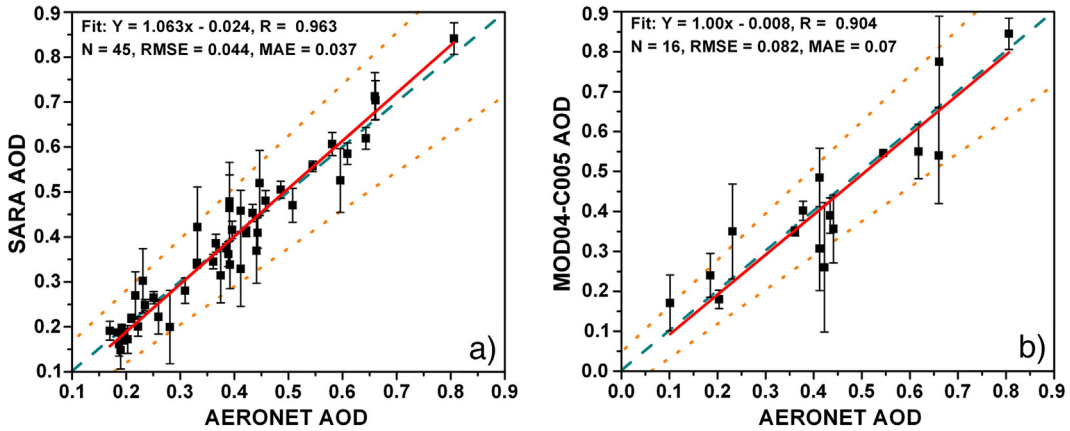

Fig. 2. Validation of (a) SARA AOD, and (b) MOD04 C005 AOD against Hok Tsui (rural) AERONET AOD from 2007 to 2009. The dotted (orange) lines, dashed (green) line, and solid (red) line are the 1:1 line, EE envelope, and regression line, respectively. (For interpretation of the references to color in this figure legend, the reader is referred to the web version of this article.)

4.1. Correlation coefficient (R)

The correlation coefficient (R) is a good indicator of agreement between Sun photometer observed AOD and satellite retrieved AOD with higher values indicating better agreement. We obtained R from Deming Regression (DR, Deming, 1943) as opposed to Linear Regression (LR, Westgard & Hunt, 1973) because DR estimates an unbiased slope by assuming the Gaussian distribution of errors in both x and y data points (which is typical of our data) (Cornbleet & Gochman, 1979; Deming, 1943; Linnet, 1993, 1998). On the other hand LR estimates a biased slope by assuming random measurement errors in the dependent variable (y) and an error free independent variable (x) (Cornbleet & Gochman, 1979; Linnet, 1993; Stöckl et al., 1998), but is inappropriate for use when significant errors are expected in both variables.

4.2. Root mean square error (RMSE)

The root mean square error (RMSE) used to measure the differences between satellite retrieved AOD and Sun photometer measured AOD is sensitive to both systematic and random errors. The RMSE can be defined as follow:

$$\mathrm{RMSE} = \sqrt{\frac{1}{n}\sum_{i=1}^{n}\left(AOD_{(satellite)i} - AOD_{(sunphotometer)i}\right)^2} \tag{12}$$

where $AOD_{satellite}$ is the satellite retrieved AOD and $AOD_{sunphotometer}$ is the Sun photometer measured AOD.

4.3. Mean absolute error (MAE)

The mean absolute error (MAE), the most natural measure of mean error magnitude (Willmott & Matsuura, 2005), is calculated as:

$$\mathrm{MAE} = \frac{1}{n}\sum_{i=1}^{n}\left|AOD_{(satellite)i} - AOD_{(sunphotometer)i}\right|. \tag{13}$$

4.4. Expected error (EE)

Expected error (EE) is used here for the confidence envelopes of the retrieval algorithm over land to evaluate the quality of SARA and C005 AOD and is defined as follows (Levy et al., 2010; Remer et al., 2008):

$$EE = \pm\left(0.05 + 0.15AOD_{sunphotometer}\right). \tag{14}$$

Good matches (quality) of satellite-retrieved (SARA and C005) AOD are reported when the satellite-retrieved AOD falls within the following envelope (Levy et al., 2010):

$$AOD_{sunphotometer} - |EE| \le AOD_{satellite} \le AOD_{sunphotometer} + |EE| \tag{15}$$

where $|EE|$ is the absolute value of expected error.

4.5. Fraction of expected error (FOE)

The fraction of expected error (FOE) is the ratio of satellite–Sun photometer ($AOD_{satellite} - AOD_{sunphotometer}$) to the absolute value of EE ($|EE|$) and can be computed as (Mi et al., 2007):

$$\mathrm{FOE} = \left(AOD_{satellite} - AOD_{sunphotometer}\right) \Big/ |EE| \tag{16}$$

Table 2
Comparison between SARA AOD and MOD04 C005 AOD from 2007 to 2009.

Location	Lat. (N)	Long. (E)	N	R	Fitted line (SARA =)	RMSE	MAE	Data within EE (%)
PolyU	22.303°	114.179°	68	0.901	1.13C005 + 0.04	0.104	0.083	72
CT	22.282°	114.158°	62	0.914	1.06C005 + 0.03	0.085	0.068	73
TW	22.372°	114.115°	62	0.926	0.98C005 + 0.03	0.067	0.054	85
TC	22.289°	114.944°	48	0.925	1.06C005 + 0.03	0.086	0.066	77
YL	22.477°	114.039°	62	0.889	1.05C005 − 0.01	0.085	0.063	81
CityU	22.340°	114.170°	20	0.941	0.94C005 + 0.01	0.051	0.046	95
HT	22.209°	114.258°	10	0.907	1.04C005 − 0.01	0.065	0.064	70
HKIA	22.317°	113.917°	06	0.929	1.32C005 + 0.07	0.159	0.137	50
TM	22.471°	114.361°	62	0.920	1.00C005 − 0.001	0.085	0.063	86

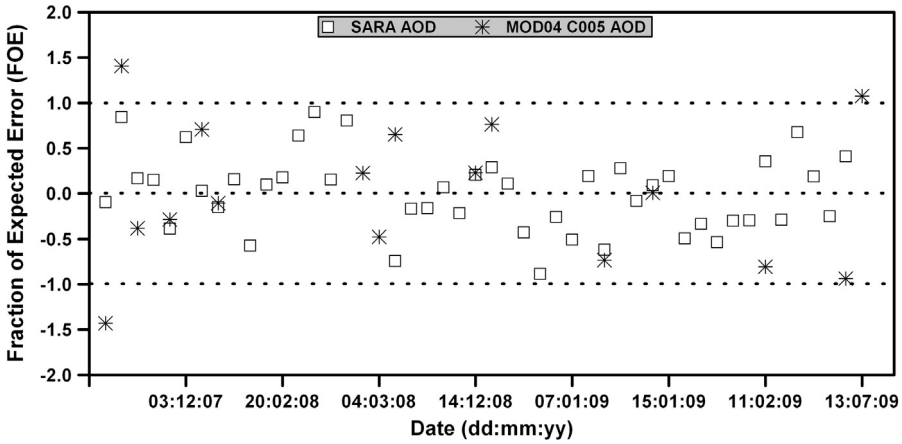

Fig. 3. Fraction of expected error (EE) in AOD retrievals of SARA and MOD04 C005 algorithms.

where $|FOE| < 1$, indicates a good match (Levy et al., 2010). Values of $FOE < 0$ and $FOE > 0$ represent underestimation and overestimation of the satellite retrievals, respectively.

5. Results

5.1. Validation with AERONET, Sky-radiometer and Microtops II AOD

Fig. 2 shows the scatter plots of SARA 500m AOD and MOD04 C005 10 km AOD with Hok Tsui AERONET AOD. In Fig. 2 the dashed (green), dotted (orange), and solid (red) lines are the 1:1 line, EE ($\pm$ 0.05 + 0.15$AOD_{sunphotometer}$) envelope line, and regression line, respectively. The SARA 500 m AOD obtained a high correlation coefficient (R = 0.963) and low values of RMSE (0.044) and MAE (0.037). Fig. 2a reveals a close correspondence between the SARA AOD and AERONET AOD, and the majority of the observations lie close to the 1:1 line. All the SARA retrieved AOD observations fall within the confidence envelope ($AOD_{sunphotometer} - |EE| \leq AOD_{satellite} \leq AOD_{sunphotometer} + |EE|$) which indicates a good quality of the retrieved AOD. The standard deviations are 0.17 and 0.16 for the SARA AOD and AERONET AOD

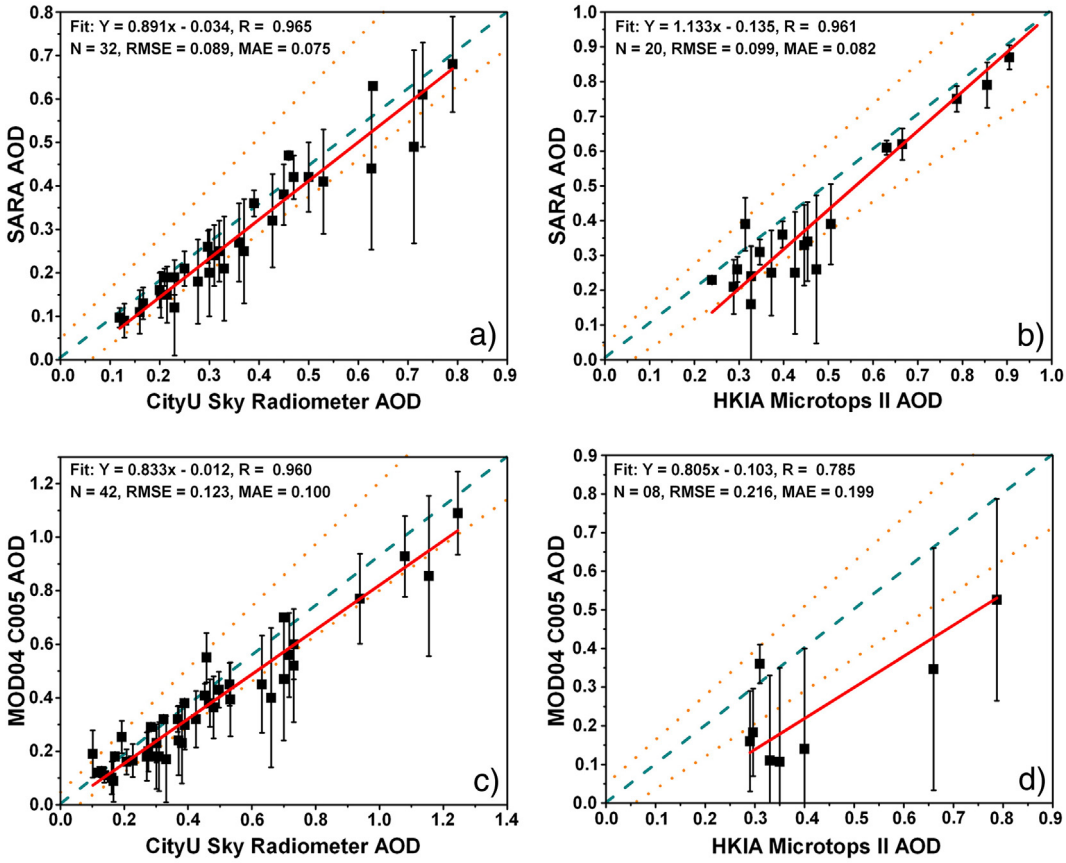

Fig. 4. Validation of SARA AOD and MOD04 C005 AOD against (a & c) CityU Sky-radiometer, and (b and d) HKIA Microtops II AOD measurements. The dotted (orange) lines, dashed (green) line, and solid (red) line are the 1:1 line, EE envelope, and regression line, respectively. (For interpretation of the references to color in this figure legend, the reader is referred to the web version of this article.)

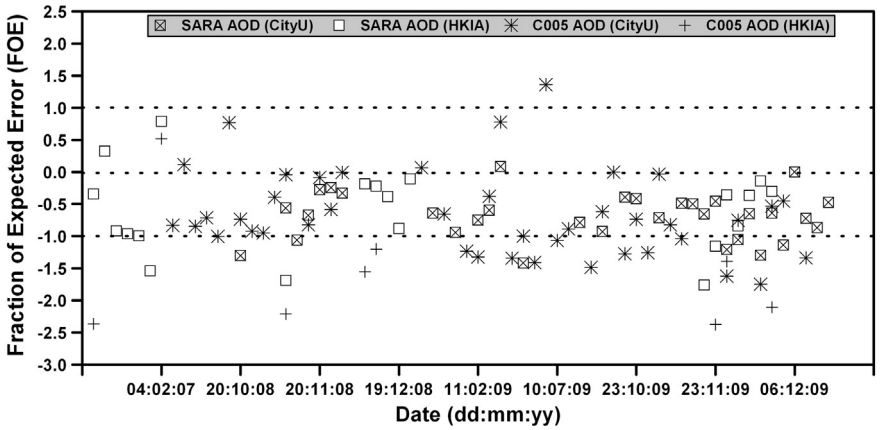

Fig. 5. Fraction of expected error (EE) in AOD retrievals of SARA and MOD04 C005 against CityU Sky-radiometer and HKIA Microtops AOD measurements.

observations, respectively, and the mean difference (SARA − AERONET) is zero. A good agreement was also observed between MOD04 C005 AOD and Hok Tsui AERONET (R = 0.904, RMSE = 0.082, and MAE = 0.070) AOD (Fig. 2b). However C005 AOD has approximately two times larger RMSE and MAE than the SARA retrieved AOD. Fig. 2b for C005 AOD shows a wide scatter of points due to underestimation and overestimation. Few observations lie close to the 1:1 line, and approximately 19% of observations fall outside the confidence envelope. The standard deviations are 0.19 and 0.19 for the C005 AOD and AERONET AOD observations respectively, and the mean difference (C005 − AERONET) is −0.01 which indicates an overall underestimation of the C005 AOD.

Approximately 81% of the FOE values from C005 AOD and 100% values from SARA AOD fall within the specified range (−1 to 1), indicating better matches (quality) of SARA AOD with AERONET than for C005 (Fig. 3). This implies that SARA AOD data is of good quality and SARA works well according to the assumptions of the surface, and the single scattering approximation.

Fig. 4a and c shows that the SARA and C005 AOD retrievals have comparable correlation coefficients (R = 0.97 and 0.96, respectively) with Sky-radiometer, having low RMSE and MAE. Approximately 80% and 67% respectively of the FOE values from SARA and C005 fall within the EE envelope for CityU Sky-radiometer respectively (Fig. 5). Slopes lower than unity indicate systematic underestimation by both SARA and MOD04 AOD retrievals. The mean differences of SARA AOD and C005 AOD from the Sky-radiometer AOD are −0.07 and −0.09 respectively, and both AOD retrievals have an error for high values of AOD. The SARA AOD achieved a higher correlation (R = 0.97) with Sky-radiometer than a previously reported Sky-radiometer study over Hong Kong (R = 0.79, Cheng et al., 2006).

Fig. 4b shows a higher correlation of the SARA AOD with the Microtops II AOD than for the C005 AOD observations (Fig. 4d). The mean differences between the SARA AOD and the C005 AOD respectively, and Microtops II AOD measurements are −0.07 and −0.19. The majority of the SARA retrieved AOD observations lie close to the 1:1 line, whereas the C005 AOD observations are very far from the line. Good agreement between satellite-retrieved AOD and Sun photometer AOD depends not only on a high correlation coefficient but also on the percentage of data falling within the EE envelope. Thus approximately 78% and 12% the FOE values from SARA AOD and C005 AOD respectively fall within the EE envelope for HKIA (Fig. 5). Fig. 5 (and 3) shows data gaps in SARA AOD due to missing PolyU (urban) AERONET AOD measurements. The SARA AOD has errors for moderate (0.3–0.5) AOD observations, whereas C005 AOD has large errors for low to high AOD observations. The MOD04 C005 AOD retrieval underestimates AOD with R = 0.79 over the Hong Kong International Airport (HKIA) which is a highly polluted area and a bright surface ($\rho_{2.21\ \mu m}$ approaching 0.25). The SARA correlation coefficient is higher (R = 0.97) than the previously developed MODIS aerosol retrieval algorithms based on LUT at 1 km (R = 0.91, Li et al., 2005) and 500 m spatial resolutions (R = 0.88, Wong et al., 2011; R = 0.83, Wang et al., 2012).

5.2. Comparison between SARA and C005 AOD

The SARA AOD data were also compared directly with C005 AOD at nine locations representing different cover types in Hong Kong for both high and low aerosol loading conditions. These locations are the Hong Kong Polytechnic University (PolyU, urban), Central (CT, urban), Tsuen Wan (TW, urban), Tung Chung (TC, suburban), Yuen Long (YL, urban), The City University of Hong Kong (CityU, suburban), Hok Tsui (HT, rural), Hong Kong International Airport (HKIA, rural), and Tap Mun (TM, rural). High correlations were achieved, with good data matches between SARA AOD and C005 AOD at all the locations except HKIA, where the correlation is high but with poor matches (only 50% data within EE = $\pm$ 0.05 $\pm$ 0.15AOD_{C005}) because, as previously noted, the C005 retrievals underestimated AOD over HKIA (Table 2). The average correlation coefficient, RMSE, and MAE are 0.917, 0.087, and 0.072, respectively, between the SARA retrieved AOD and the C005 AOD observations over Hong Kong. These comparisons imply that SARA has as good or better ability to retrieve

Table 3a
Descriptive statistics of the SARA AOD and Hok Tsui AERONET AOD.

Variable	Mean	SE mean	StDev	Minimum	Median	Maximum
AERONET	0.383	0.023	0.155	0.170	0.389	0.806
SARA AOD	0.383	0.025	0.165	0.148	0.369	0.841
$\omega_o + 0.05\omega_o$	0.365	0.023	0.157	0.141	0.352	0.801
$\omega_o - 0.05\omega_o$	0.403	0.026	0.174	0.156	0.389	0.886
$g + 0.02g$	0.405	0.029	0.195	0.134	0.373	1.128
$g - 0.02g$	0.367	0.023	0.157	0.134	0.350	0.685
$\rho_s + 0.02\rho_s$	0.434	0.024	0.164	0.198	0.418	0.876
$\rho_s - 0.02\rho_s$	0.434	0.024	0.164	0.198	0.418	0.876

Table 3b
Descriptive statistics of the SARA AOD and CityU Sky-radiometer AOD.

Variable	Mean	SE mean	StDev	Minimum	Median	Maximum
Sky-radiometer	0.372	0.032	0.183	0.119	0.325	0.790
SARA AOD	0.297	0.029	0.163	0.090	0.250	0.680
$\omega_o + 0.05\omega_o$	0.283	0.0274	0.155	0.086	0.238	0.648
$\omega_o - 0.05\omega_o$	0.313	0.030	0.172	0.095	0.263	0.716
$g + 0.02g$	0.327	0.034	0.191	0.100	0.265	0.730
$g - 0.02g$	0.290	0.028	0.161	0.100	0.245	0.680
$\rho_s + 0.02\rho_s$	0.375	0.029	0.165	0.160	0.325	0.740
$\rho_s - 0.02\rho_s$	0.375	0.029	0.165	0.160	0.325	0.740

Table 3c
Descriptive statistics of the SARA AOD and HKIA Microtops II AOD.

Variable	Mean	SE mean	StDev	Minimum	Median	Maximum
Microtops II	0.501	0.050	0.223	0.239	0.436	0.968
SARA AOD	0.433	0.057	0.253	0.160	0.335	1.030
$\omega_o + 0.05\omega_o$	0.412	0.054	0.241	0.152	0.319	0.981
$\omega_o - 0.05\omega_o$	0.455	0.060	0.266	0.168	0.353	1.084
$g + 0.02g$	0.470	0.069	0.360	0.150	0.350	1.150
$g - 0.02g$	0.422	0.054	0.241	0.150	0.350	1.060
$\rho_s + 0.02\rho_s$	0.509	0.056	0.251	0.260	0.415	1.150
$\rho_s - 0.02\rho_s$	0.509	0.056	0.251	0.260	0.415	1.150

accurate AOD over different land cover types during both high and low aerosol loading conditions.

5.3. Sensitivity analysis

To confirm the robustness of the SARA methodology, a sensitivity analysis of the SARA AOD was undertaken by increasing/decreasing by 5% the value of SSA ($\omega_o \pm 0.05\omega_o$), and by 2% the values of asymmetry parameter ($g \pm 0.02g$) and the surface reflectance ($\rho_s \pm 0.02\rho_s$). The descriptive statistics used are mean, standard error of mean (SE mean), standard deviation (StDev), minimum, median and maximum of the Hok Tsui AERONET, CityU Sky-radiometer, and HKIA Microtops II Sun photometers and the SARA AOD observations (Tables 3a, 3b and 3c). The $\omega_o \pm 0.05\omega_o$, $g \pm 0.02g$ and $\rho_s \pm 0.02\rho_s$ are the new retrieved SARA AOD by increasing/decreasing the SSA, g and ρ_s values, respectively. The statistics show that the mean SARA retrieved AOD differences range from −2% to 2%, −2% to 4%, and 5% to 8% by increasing/decreasing the SSA (5%), g (2%) and ρ_s (2%) values respectively. These results suggest that SARA retrieved AOD is more sensitive to ρ_s than to g and SSA.

5.4. Spatial–temporal pattern of AOD

Fig. 6a shows the spatial distribution of SARA AOD over Hong Kong and Pearl River Delta (PRD) region on 30th January 2007. It reveals a high aerosol loading event (black circle) over PRD region due to emissions from local power plants and industries and provides detailed information on pollution sources. A higher value of SARA AOD (~0.80) was observed over PRD than over Hong Kong (AOD ~ 0.65). However, the C005 AOD retrieval was unable to depict the high pollution event and shows missing pixels over the affected area (Fig. 6b), where it is suspected that high aerosol reflectance resulted in many 500 m pixels within the 10 km kernel failing the selection criteria in the MODIS visible channel (0.66 μm). The SARA AOD is thus judged to be more suitable than C005 AOD to represent the spatial pattern of aerosols over the complex and hilly terrain of Hong Kong as well as the industrialized area of PRD. The SARA AOD image overlaid with the road network of Kowloon and Hong Kong Island (Fig. 6c) shows the ability of the SARA AOD to identify local emission sources especially over the

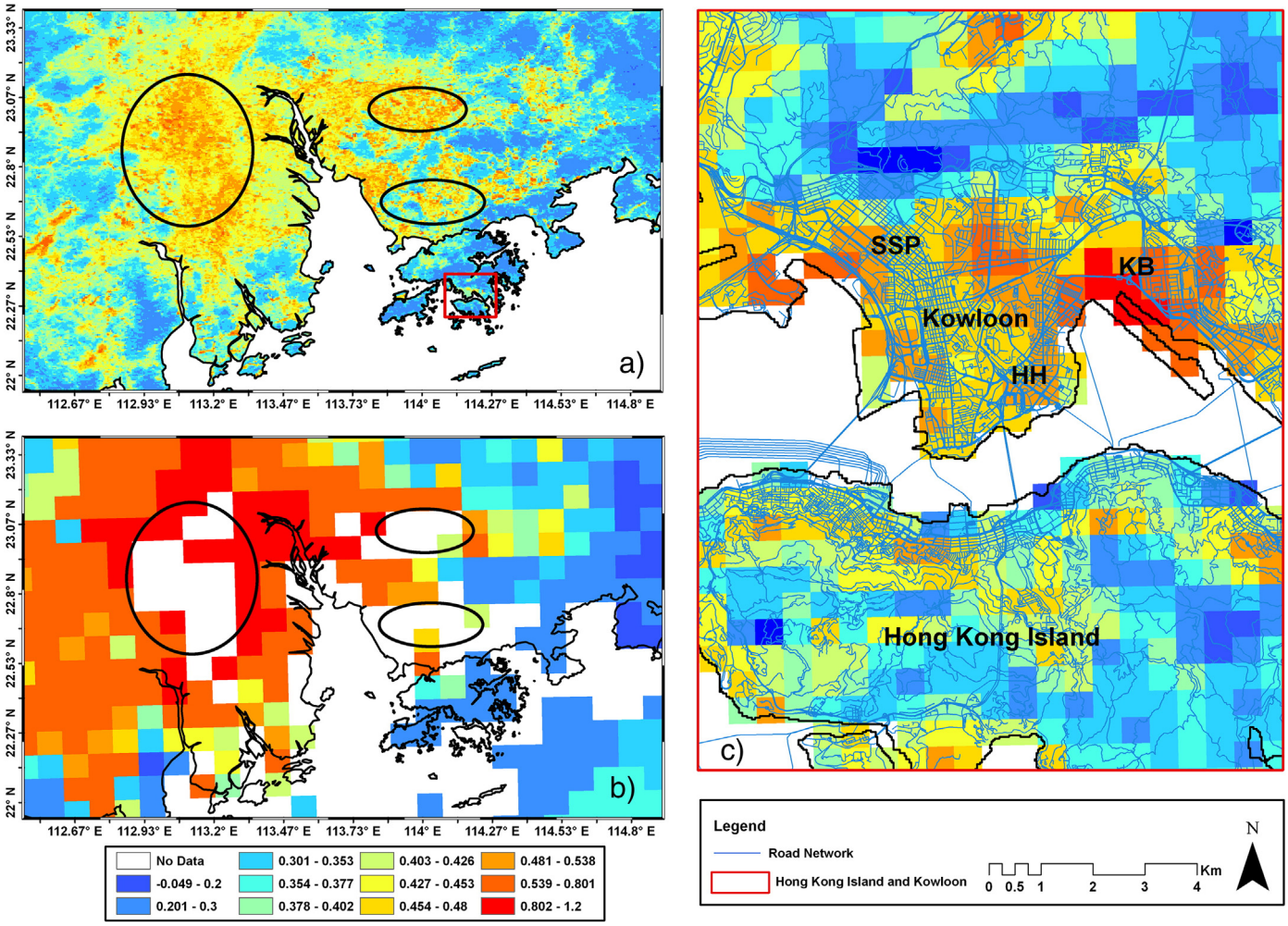

Fig. 6. Spatial pattern of SARA (a), and C005 (b) AOD for a high aerosol loading event (30th January 2007) over the Pearl River Delta (PRD) region and Hong Kong. Also shown, in panel (c), is the SARA AOD under-laid with road data over Kowloon and Hong Kong Island.

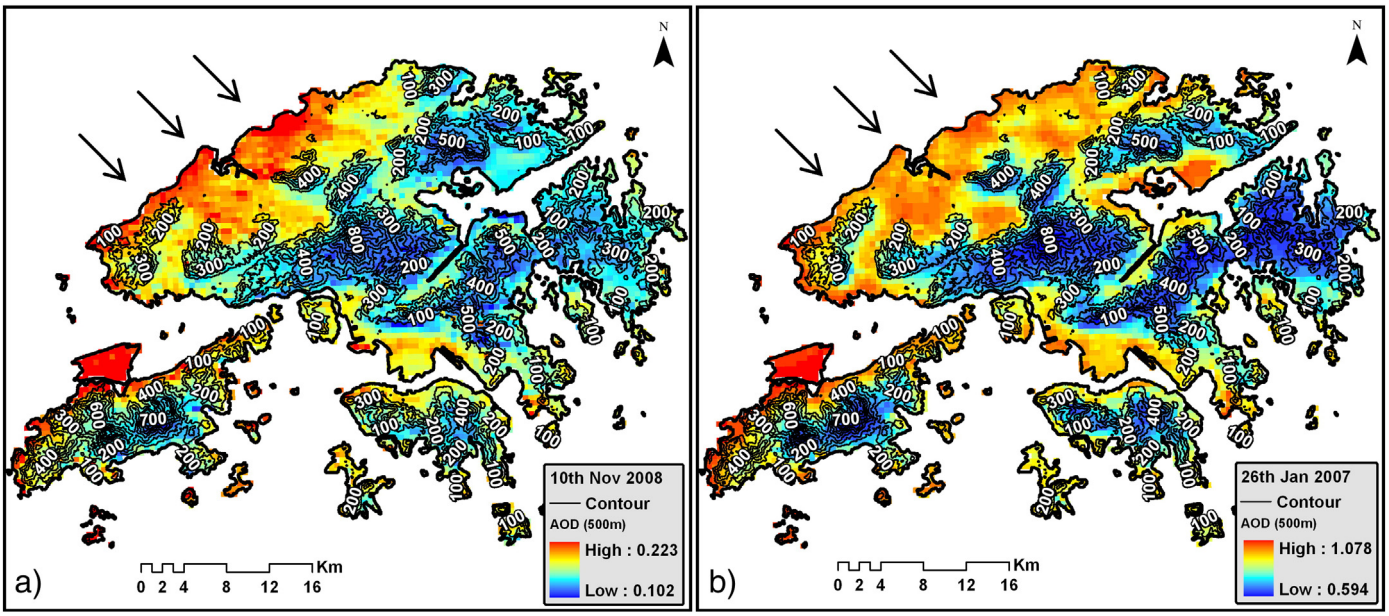

Fig. 7. Variations in AOD between hilly and urban regions of Hong Kong on (a) low (10th November 2008), and (b) high (26th January 2007) aerosol loading conditions.

dense and congested districts of Kowloon Bay (KB), Hung Hom (HH), Sham Shui Po (SSP), and North Hong Kong Island.

Fig. 7 shows a sharp boundary in AOD values between urban and hilly regions of Hong Kong, indicating greater variations between urban and hilly areas than between urban and rural areas during both high and low aerosol loading conditions. Steep mountain slopes create a blocking effect, and this combined with a boundary layer height often lower than the mountains, traps pollutants in the lowlands. Therefore AOD has a strong relationship with elevation and high values of AOD are usually observed at lower elevations (<100 m) which correspond to urban, suburban and rural regions in Hong Kong. The northwest border of Hong Kong adjacent to the industrial city of Shenzhen on the Chinese Mainland (arrowed in Fig. 7) is a mainly rural, lowland area, and shows high AOD values on both dates.

In spite of large spatial differences, remarkably similar temporal trends of AOD were observed across urban (PolyU), rural (Tap Mun) and hilly (Tai Mo Shan) regions of Hong Kong (Fig. 8). This suggests that much of the air pollution in Hong Kong is due to regional factors because if pollution was mainly local (such as urban vehicle emissions) then urban/rural temporal trends would be out of phase, unlike the close temporal correspondence shown Fig. 8. Fig. 8 also indicates that the C005 retrievals overestimate AOD over hilly area (elevation ~957 m) due to their coarse resolution as 10 km pixels cover both high and low elevations in the same pixel retrieving the same AOD

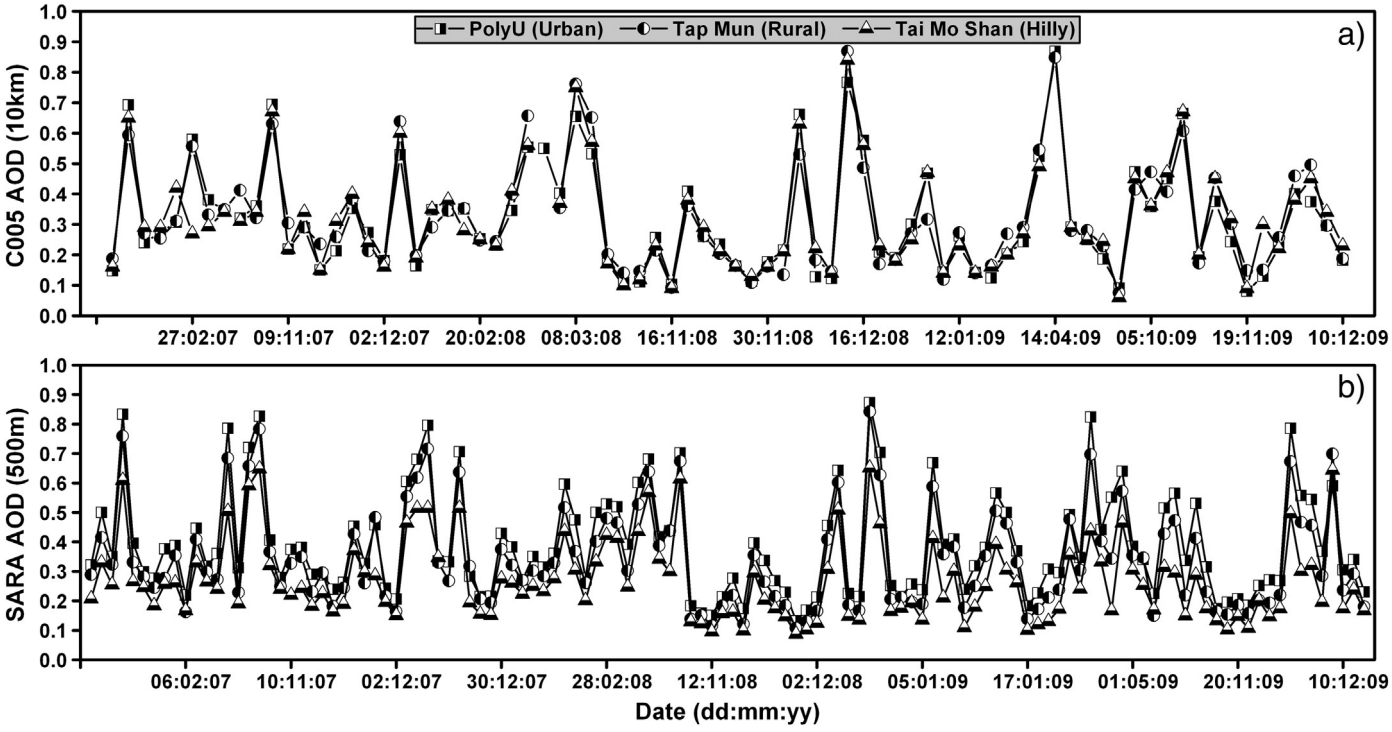

Fig. 8. Temporal trends of (a) MOD04 AOD, and (b) SARA AOD from 2007 to 2009.

values over both. However, the SARA retrievals, because of better spatial resolution, are better able to represent AOD values over each distinct region.

6. Conclusion

A Simplified MODIS Aerosol Retrieval Algorithm (SARA) at 500 m spatial resolution was developed using MODIS data products (MOD02HKM, MOD03 and MOD09GA), assuming Lambertian surfaces, single scattering approximation, and that single scattering albedo and asymmetry factors are regionally constant for a particular day. Validation with three different Sun photometers located in different land cover types of Hong Kong indicated that:

1. The SARA retrieved AOD is able to represent the true picture of aerosol loadings over the complex and hilly terrain of Hong Kong.
2. The MOD04 C005 AOD retrievals are inferior to SARA AOD retrievals and underestimate AOD over the Hong Kong International Airport (HKIA) which is a highly polluted area with bright surface ($\rho_{2.21\ \mu m}$ approaching 0.25). The C005 retrievals also overestimated the AOD over areas of high elevation.
3. The SARA AOD because of its higher spatial resolution can identify detailed pollution sources in the PRD region, whereas the C005 AOD retrieval is unable to depict pollution sources due to low resolution, as well as the effect of bright aerosols on the visible band thresholding, resulting in missing data.
4. AOD values have a similar temporal trend over different land cover types of Hong Kong, indicating more contribution from regional than local pollution sources.
5. AOD has little variation between urban and rural areas but has more variation between urban and upland areas. High values and maximum concentrations of AOD were observed at lower elevations (approximately <100m) areas and low values of AOD are associated with hilly terrain.
6. Overall, the SARA AOD has a better agreement with ground-based Sun photometers than does the C005 AOD and is more suitable to retrieve AOD over mixed surfaces of Hong Kong during both high and low aerosol loading conditions.

Acknowledgment

The authors would like to acknowledge NASA Goddard Space Flight Center for MODIS sensor data. We also would like to thank Dr. Brent Holben for helping with the AERONET stations in Hong Kong and the reviewers for their valuable suggestions and comments that have greatly improved the quality of the paper. Grants PolyU5253/10E and GYJ76 sponsored this research. Additional support was provided by the New Mexico State University Agricultural Experiment Station. Dr. P.W. Chan of the Hong Kong Observatory provided the CityU and HKIA AOD data used in this study.

Appendix A. Supplementary data

Supplementary data associated with this article can be found in the online version, at http://dx.doi.org/10.1016/j.rse.2013.04.014. These data include Google maps of the most important areas described in this article.

References

Ångström, A. (1930). On the atmospheric transmission of sun radiation II. *Geografiska Annaler*, *12*, 130–159.
Ångström, A. (1964). The parameters of atmospheric turbidity. *Tellus*, *16*, 64–75.
Antoine, D., & Morel, A. (1998). Relative importance of multiple scattering by air molecules and aerosols in forming the atmospheric path radiance in the visible and near-infrared parts of the spectrum. *Applied Optics*, *37*, 2245–2259.
Campanelli, M., Nakajima, T., & Olivieri, B. (2004). Determination of the solar calibration constant for a sun-sky radiometer: Proposal of an in-situ procedure. *Applied Optics*, *43*, 651–659.
Chan, C. K., & Yao, X. (2008). Air pollution in mega cities in China. *Atmospheric Environment*, *42*, 1–42.
Che, H., Shi, G., Uchiyama, A., Yamazaki, A., Chen, H., Goloub, P., et al. (2008). Intercomparison between aerosol optical properties by a PREDE skyradiometer and CIMEL sunphotometer over Beijing, China. *Atmospheric Chemistry and Physics*, *8*, 3199–3214.
Cheng, A. Y. S., Chan, M. H., & Yang, X. (2006). Study of aerosol optical thickness in Hong Kong, validation, results, and dependence on meteorological parameters. *Atmospheric Environment*, *40*, 4469–4477.
Clarke, A. D., Collins, W. G., Rasch, P. J., Kapustin, V. N., Moore, K., Howell, S., et al. (2001). Dust and pollution transport on global scales: Aerosol measurements and model predictions. *Journal of Geophysical Research*, *106*, 32555–32569.
Cornbleet, P. J., & Gochman, N. (1979). Incorrect least-squares regression coefficients in method-comparison analysis. *Clinical Chemistry*, *25*, 432–438.
Deming, W. E. (1943). Statistical adjustment of data. New York: Dover Publications.
Duffie, J. A., & Beckman, W. A. (1991). Solar engineering of thermal processes (3rd ed.). New York: Wiley.
Gordon, H. R., & Wang, M. (1994). Retrieval of water-leaving radiance and aerosol optical thickness over the oceans with SeaWiFS: A preliminary algorithm. *Applied Optics*, *33*, 443–452.
Hauser, A., Oesch, D., Foppa, N., & Wunderle, S. (2005). NOAA AVHRR derived aerosol optical depth over land. *Journal of Geophysical Research*, *110*, D08204. http://dx.doi.org/10.1029/2004JD005439.
Herman, M., Deuzé, J. L., Devaux, C., Goloub, P., Bréon, F. M., & Tanré, D. (1997). Remote sensing of aerosols over land surfaces including polarization measurements and application to POLDER measurements. *Journal of Geophysical Research*, *102*, 17039–17049.
Holben, B. N., Eck, T. F., Slutsker, I., Tanré, D., Buis, J. P., Setzer, A., et al. (1998). AERONET a federated instrument network and data archive for aerosol characterization. *Remote Sensing of Environment*, *66*, 1–16.
Holben, B. N., Tanré, D., Smirnov, A., Eck, T. F., Slutsker, I., Abuhassan, N., et al. (2001). An emerging ground-based aerosol climatology: Aerosol optical depth from AERONET. *Journal of Geophysical Research*, *106*, 12067–12097.
Hsu, N. C., Tsay, S. -C., King, M. D., & Herman, J. R. (2004). Aerosol properties over bright reflecting source regions. *IEEE Transactions on Geoscience and Remote Sensing*, *42*, 557–569.
Hsu, N. C., Tsay, S. -C., King, M. D., & Herman, J. R. (2006). Deep blue retrievals of Asian aerosol properties during ACE-Asia. *IEEE Transactions on Geoscience and Remote Sensing*, *44*, 3180–3195.
Hubanks, P., Chu, A., Ridgway, B., Strabala, K., Platnick, S., Mattoo, S., et al. (2012). *MODIS atmosphere QA plan for Collection 005 and 051 (includes cirrus flag & high cloud flag (06_CT) clarification, deep blue aerosol update, aerosol over land update, water vapor and atmosphere profile update, changes to MOD35 QA bit field documentation) version 3.10, 2013.*
Hyer, E. J., Reid, J. S., & Zhang, J. (2011). An over-land aerosol optical depth data set for data assimilation by filtering, correction, and aggregation of MODIS Collection 5 optical depth retrievals. *Atmospheric Measurement Techniques*, *4*, 379–408.
Ichoku, C., Levy, R., Kaufman, Y. J., Remer, L. A., Li, R. R., Martins, V. J., et al. (2002). Analysis of the performance characteristics of the five-channel Microtops II Sun photometer for measuring aerosol optical thickness and precipitable water vapor. *Journal of Geophysical Research*, *107*(D13), 4179.
Jethva, H., Satheesh, S. K., & Srinivasan, J. (2007). Assessment of second-generation MODIS aerosol retrieval (Collection 005) at Kanpur, India. *Geophysical Research Letters*, *34*(19), L19802. http://dx.doi.org/10.1029/2007GL029647.
Kahn, R. A., Gaitley, B. J., Garay, M. J., Diner, D. J., Eck, T. F., Smirnov, A., et al. (2010). Multiangle Imaging SpectroRadiometer global aerosol product assessment by comparison with the Aerosol Robotic Network. *Journal of Geophysical Research*, *115*, D23209. http://dx.doi.org/10.1029/2010JD014601.
Kahn, R., Gaitley, B., Martonchik, J., Diner, D., Crean, K., & Holben, B. (2005). Multiangle Imaging Spectroradiometer (MISR) global aerosol optical depth validation based on two years of coincident Aerosol Robotic Network (AERONET) observations. *Journal of Geophysical Research*, *110*.
Kaufman, Y. J., Tanre, D., & Boucher, O. (2002). A satellite view of aerosols in the climate system. *Nature*, *419*, 215–223.
Kaufman, Y. J., Tanré, D., Gordon, H. R., Nakajima, T., Lenoble, J., Frouin, R., et al. (1997a). Passive remote sensing of tropospheric aerosol and atmospheric correction for the aerosol effect. *Journal of Geophysical Research*, *102*(14), 16815–16830.
Kaufman, Y. J., Tanré, D., Remer, L. A., Vermote, E. F., Chu, A., & Holben, B. N. (1997b). Operational remote sensing of tropospheric aerosol over land from EOS moderate resolution imaging spectroradiometer. *Journal of Geophysical Research*, *102*(14), 17051–17067.
Kelley, C. T. (1995). Iterative methods for linear and nonlinear equations. Society for Industrial and Applied Mathematics.
King, M. D., Kaufman, Y. J., Tanré, D., & Nakajima, J. (1999). Remote sensing of tropospheric aerosols from space: Past, present and future. *Bulletin of the American Meteorological Society*, *80*, 2229–2259.
Knobelspiesse, K. D., Pietras, C., Fargion, G. S., Wang, M., Frouin, R., Miller, M. A., et al. (2004). Maritime aerosol optical thickness measured by handheld sun photometers. *Remote Sensing of Environment*, *93*, 87–106.
Kokhanovsky, A., & Leeuw, G. D. (2009). Satellite aerosol remote sensing over land (Springer Praxis Books/Environmental Sciences). Springer.
Lado-Bordowsky, O., & Naour, I. (1997). Optical paths involved in determining the scattering angle for the scattering algorithm developed in LOWTRAN7. *International Journal of Infrared and Millimeter Waves*, *18*, 1689–1696.

Levy, R. C., Remer, L. A., & Dubovik, O. (2007b). Global aerosol optical properties and application to Moderate Resolution Imaging Spectroradiometer aerosol retrieval over land. *Journal of Geophysical Research*, *112*(13), 1–15.

Levy, R. C., Remer, L. A., Kleidman, R. G., Mattoo, S., Ichoku, C., Kahn, R., et al. (2010). Global evaluation of the Collection 5 MODIS dark-target aerosol products over land. *Atmospheric Chemistry and Physics Discussions*, *10*, 14815–14873.

Levy, R. C., Remer, L. A., Mattoo, S., Vermote, E. F., & Kaufman, Y. J. (2007a). Second generation operational algorithm: Retrieval of aerosol properties over land from inversion of Moderate Resolution Imaging Spectroradiometer spectral reflectance. *Journal of Geophysical Research*, *112*(13), 1–21.

Li, C., Lau, A. K. -H., Mao, J., & Chu, D. A. (2005). Retrieval, validation, and application of the 1-km aerosol optical depth from MODIS measurements over Hong Kong. *IEEE Transactions on Geoscience and Remote Sensing*, *43*, 2650–2658.

Li, Z., Niu, F., Lee, K. -H., Xin, J., Hao, W. M., Nordgren, B., et al. (2007). Validation and understanding of Moderate Resolution Imaging Spectroradiometer aerosol products (C5) using ground-based measurements from the handheld Sun photometer network in China. *Journal of Geophysical Research*, *112*(22), 1–16.

Li, Z., Zhao, X., Kahn, R., Mishchenko, M., Remer, L., Lee, K. -H., et al. (2009). Uncertainties in satellite remote sensing of aerosols and impact on monitoring its long-term trend: A review and perspective. *Annales Geophysicae*, *27*, 2755–2770.

Liang, S. (2005). Quantitative remote sensing of land surfaces. New Jersey: John Wiley & Sons, Inc.

Linnet, K. (1993). Evaluation of regression procedures for methods comparison studies. *Clinical Chemistry*, *39*, 424–432.

Linnet, K. (1998). Performance of Deming regression analysis in case of misspecified analytical error ratio in method comparison studies. *Clinical Chemistry*, *44*, 1024–1031.

Liu, Y., Huang, J., Shi, G., Takamura, T., Khatri, P., Bi, J., et al. (2011). Aerosol optical properties and radiative effect determined from sky-radiometer over Loess Plateau of Northwest China. *Atmospheric Chemistry and Physics*, *11*, 11455–11463.

Mi, W., Li, Z., Xia, X., Holben, B., Levy, R., Zhao, F., et al. (2007). Evaluation of the Moderate Resolution Imaging Spectroradiometer aerosol products at two Aerosol Robotic Network stations in China. *Journal of Geophysical Research*, *112*(22), 1–14.

Mishchenko, M. I., Geogdzhayev, I. V., Cairns, B., Rossow, W. B., & Lacis, A. A. (1999). Aerosol retrievals over the ocean by use of channels 1 and 2 AVHRR data: Sensitivity analysis and preliminary results. *Applied Optics*, *38*(36), 7325–7341.

Morys, M., Mims, F. M., Hagerup, S., Anderson, S. E., Baker, A., Kia, J., et al. (2001). Design, calibration, and performance of MICROTOPS II handheld ozone monitor and Sun photometer. *Journal of Geophysical Research*, *106*, 14573–14582.

Nakajima, T., Tonna, G., Rao, R., Boi, P., Kaufman, Y. J., & Holben, B. N. (1996). Use of sky brightness measurements from ground for remote sensing of particulate polydispersions. *Applied Optics*, *35*, 2672–2686.

North, P. R. J. (2002). Estimation of aerosol opacity and land surface bidirectional reflectance from ATSR-2 dual-angle imagery: Operational method and validation. *Journal of Geophysical Research*, *107*, 4149.

Papadimas, C. D., Hatzianastassiou, N., Mihalopoulos, N., Kanakidou, M., Katsoulis, B. D., & Vardavas, I. (2009). Assessment of the MODIS Collections C005 and C004 aerosol optical depth products over the Mediterranean basin. *Atmospheric Chemistry and Physics*, *9*, 2987–2999.

Prados, A. I., Kondragunta, S., Ciren, P., & Knapp, K. R. (2007). GOES Aerosol/Smoke Product (GASP) over North America: Comparisons to AERONET and MODIS observations. *Journal of Geophysical Research*, *112*, D15201.

Rahman, H., Pinty, B., & Verstraete, M. M. (1993). Coupled surface-atmosphere reflectance (CSAR) model: 2. Semiempirical surface model usable with NOAA advanced very high resolution radiometer data. *Journal of Geophysical Research*, *98*(11), 20791–20801.

Remer, L. A., Chin, M., DeCola, P., Feingold, G., Halthore, R., Kahn, R. A., et al. (2009). Executive summary. In M. Chin, R. A. Kahn, & S. E. Schwartz (Eds.), *Atmospheric aerosol properties and climate impacts* (pp. 1–8). U.S. Climate Change Science Program.

Remer, L. A., Kaufman, Y. J., Tanré, D., Mattoo, S., Chu, D. A., Martins, J. V., et al. (2005). The MODIS aerosol algorithm, products, and validation. *Journal of the Atmospheric Sciences*, *62*(4), 947–973.

Remer, L. A., Kleidman, R. G., Levy, R. C., Kaufman, Y. J., Tanré, D., Mattoo, S., et al. (2008). Global aerosol climatology from the MODIS satellite sensors. *Journal of Geophysical Research*, *113113*, D14S07. http://dx.doi.org/10.1029/2007JD009661.

Riffler, M., Popp, C., Hauser, A., Fontana, F., & Wunderle, S. (2010). Validation of a modified AVHRR aerosol optical depth retrieval algorithm over Central Europe. *Atmospheric Measurement Techniques*, *3*, 1255–1270.

Salomonson, V. V., Barnes, W., & Masuoka, E. J. (2006). Introduction to MODIS and an overview of associated activities. *Earth Science Satellite Remote Sensing*, *1*. (pp. 12–32). Heidelberg: Springer-Verlag Berlin Heidelberg.

Sayer, A. M., Hsu, N. C., Bettenhausen, C., Jeong, M. -J., Holben, B. N., & Zhang, J. (2012). Global and regional evaluation of over-land spectral aerosol optical depth retrievals from SeaWiFS. *Atmospheric Measurement Techniques*, *5*, 1761–1778.

Smirnov, A., Holben, B. N., Eck, T. F., Dubovik, O., & Slutsker, I. (2000). Cloud-screening and quality control algorithms for the AERONET database. *Remote Sensing of Environment*, *73*, 337–349.

Stöckl, D., Dewitte, K., & Thienpont, L. M. (1998). Validity of linear regression in method comparison studies: Is it limited by the statistical model or the quality of the analytical input data? *Clinical Chemistry*, *44*(11), 2340–2346.

Tang, J., Xue, Y., Yu, T., & Guan, Y. (2005). Aerosol optical thickness determination by exploiting the synergy of TERRA and AQUA MODIS. *Remote Sensing of Environment*, *94*, 327–334.

Tanré, D., Deschamps, P. Y., Devaux, C., & Herman, M. (1988). Estimation of Saharan aerosol optical thickness from blurring effects in thematic mapper data. *Journal of Geophysical Research*, *93*(12), 15955–15964.

Tanré, D., Herman, M., Deschamps, P. Y., & Leffe, A. d. (1979). Atmospheric modeling for space measurements of ground reflectances, including bidirectional properties. *Applied Optics*, *18*(21), 3587–3594.

Tasumi, M., Allen, R. G., & Trezza, R. (2008). At-surface reflectance and albedo from satellite for operational calculation of land surface energy balance. *Journal of Hydrologic Engineering*, *13*, 51–63.

Torres, O., Bhartia, P. K., Herman, J. R., Sinyuk, A., Ginoux, P., & Holben, B. (2002). A long term record of aerosol optical depth from TOMS observations and comparison to AERONET measurements. *Journal of the Atmospheric Sciences*, *59*, 398–413.

Torres, O., Tanskanen, A., Veihelmann, B., Ahn, C., Braak, R., Bhartia, P. K., et al. (2007). Aerosols and surface UV products from Ozone Monitoring Instrument observations: An overview. *Journal of Geophysical Research*, *112*, D24S47.

Tsang, H., Kwok, R., & Miguel, A. H. (2008). Pedestrian exposure to ultrafine particles in Hong Kong under heavy traffic conditions. *Aerosol and Air Quality Research*, *8*, 19–27.

van de Hulst, H. C. (1948). Scattering in a planetary atmosphere. *The Astrophysical Journal*, *107*, 220–246.

Vermote, E. F., & Kotchenova, S. (2008). Atmospheric correction for the monitoring of land surfaces. *Journal of Geophysical Research*, *113*(23), 1–12.

Vermote, E. F., Tanre, D., Deuze, J. L., Herman, M., & Morcette, J. J. (1997). Second simulation of the satellite signal in the solar spectrum, 6S: An overview. *IEEE Transactions on Geoscience and Remote Sensing*, *35*, 675–686.

Vidot, J., Santer, R., & Aznay, O. (2008). Evaluation of the MERIS aerosol product over land with AERONET. *Atmospheric Chemistry and Physics*, *8*, 7603–7617.

Wang, Y., Xue, Y., Li, Y., Guang, J., Mei, L., Xu, H., et al. (2012). Prior knowledge-supported aerosol optical depth retrieval over land surfaces at 500 m spatial resolution with MODIS data. *International Journal of Remote Sensing*, *33*, 674–691.

Westgard, J. O., & Hunt, M. R. (1973). Use and interpretation of common statistical tests in method-comparison studies. *Clinical Chemistry*, *19*, 49–57.

Willmott, C., & Matsuura, K. (2005). Advantages of the mean absolute error (MAE) over the root mean square error (RMSE) in assessing average model performance. *Climate Research*, *30*, 79–82.

Wong, M. S., Nichol, J. E., & Lee, K. H. (2011). An operational MODIS aerosol retrieval algorithm at high spatial resolution, and its application over a complex urban region. *Atmospheric Research*, *99*, 579–589.

Xue, Y., & Cracknell, A. P. (1995). Operational bi-angle approach to retrieve the Earth surface albedo from AVHRR data in the visible band. *International Journal of Remote Sensing*, *16*, 417–429.